Sensors & Actuators: B. Chemical 282 (2019) 896–903

Contents lists available at ScienceDirect

Sensors and Actuators B: Chemical

journal homepage: www.elsevier.com/locate/snb

Probing NAD^+/NADH-dependent biocatalytic transformations based on oxidase mimics of MnO_2

Shuyun Zhu[a,*], Cuihua Lei[a], Jing Sun[b], Xian-En Zhao[a,*], Xiao Wang[c], Xiaolu Yan[a], Wei Liu[c], Hua Wang[a,*]

[a] College of Chemistry and Chemical Engineering, Qufu Normal University, Qufu City, Shandong Province, 273165, China
[b] Qinghai Key Laboratory of Qinghai-Tibet Plateau Biological Resources, Northwest Institute of Plateau Biology, Chinese Academy of Sciences, Xining City, Qinghai Province, 810001, China
[c] Shandong Key Laboratory of TCM Quality Control Technology, Shandong Analysis and Test Center, Qilu University of Technology (Shandong Academy of Sciences), 19 Keyuan Street, Jinan, 250014, China

ARTICLE INFO

Keywords:
MnO_2 nanosheets
Artificial oxidase
Colorimetric assay
NADH
Ethanol
Pyruvic acid

ABSTRACT

In the present study, a novel colorimetric sensing platform was constructed for probing the NAD^+/NADH-dependent biocatalytic transformations. Manganese dioxide (MnO_2) nanosheets as an oxidase-mimicking nanomaterial could directly oxidize 3,3′,5,5′-tetramethylbenzidine (TMB) into oxTMB without the need of H_2O_2. Importantly, it was found that NADH could easily trigger the decomposition of MnO_2 nanosheets, causing the decrease of solution absorbance. This is demonstrated by the enzyme catalysis reactions of two dehydrogenase models, ethanol dehydrogenase (ADH) and lactate dehydrogenase (LDH), where NADH is formed and consumed, respectively, in their physiological enzymatic reactions. A MnO_2-TMB sensing platform was thereby proposed for the analysis of their catalytic reaction substrates including ethanol and pyruvic acid. The detection limits of ethanol and pyruvic acid can reach 5.0 μM and 100 nM, respectively. The developed optical biosensing platform can be used to develop other dehydrogenase-based biosensors followed by monitoring their substrates.

1. Introduction

Enzymes as a kind of biological catalysts play a crucial role in the process of biocatalytic transformation [1]. Nicotinamide adenine dinucleotide (NADH) and its oxidized form nicotinamide adenine dinucleotide (NAD^+) play an important role as cofactor in numerous biocatalytic processes, including energy metabolism, mitochondrial responses, immunological functions, aging and cell death [2]. Increasing evidence has also suggested that NADH metabolism is potential therapeutic target for treating several neurological disorders. NADH and NAD^+ transfer hydrogen atoms and electrons from one metabolite to another in many cellular redox reactions. Because over 300 dehydrogenases require NADH and NAD^+ as the cofactors, therefore the appropriate probing NADH or NAD^+ could provide an effective method to detect $NAD(H)^+$-dependent enzymes, as well as to detect their substrates [3,4].

Advances in nanoscience and nanotechnology, nanomaterials find growing interest for probing various biocatalytic transformations or proteins and biologically relevant small molecules [5–9]. There are many reports where nanomaterials have been used to monitor the NAD^+/NADH-dependent enzyme biocatalytic processes by optical and electrochemical analysis methods [10–16]. Electrochemical sensing methods suffer from multiple drawbacks like electrode fouling and requirement of over-potential to oxidize NADH to NAD^+ leading to non-specific oxidation and high cross reactivity [11]. To overcome this problem, many studies have focused on the optical detections of dehydrogenase mediated reactions through the detection of NADH or NAD^+ [12,11–16]. For example, gold nanoparticles (AuNPs) were employed for the optical detection of NADH and probing the NAD^+-dependent dehydrogenase transformation [12,13]. Semiconductor quantum dots (QDs), as fluorescent labels, also find growing interest in the development of biosensors based on NADH/NAD^+-dependent biocatalysts [14,15]. Moreover, fluorescent silver nanoclusters (AgNCs) have been developed for the quantitative detection of NAD^+ and monitoring NAD^+/NADH based enzymatic reactions [16]. However, most of these nanomaterials might suffer from some drawbacks, such as laborious synthesis procedure for QDs, high cost for AuNPs and AgNCs. In addition, the aggregation process of AuNPs analysis is easy to be affected by some environmental stimuli such as salt of high concentration and longtime incubation, which may reduce the accuracy.

* Corresponding authors.
E-mail addresses: shuyunzhu1981@163.com (S. Zhu), xianenzhao@163.com (X.-E. Zhao), huawangqfnu@126.com (H. Wang).

https://doi.org/10.1016/j.snb.2018.11.140
Received 24 April 2018; Received in revised form 23 November 2018; Accepted 28 November 2018
Available online 28 November 2018
0925-4005/

Thus, it is still highly desirable to develop new optical assays for probing NADH/NAD^+-dependent bio-catalyzed transformation.

It is well established that 3,3′,5,5′-tetramethylbenzidine (TMB)-based optical assay is employed as an effective and easy-to-use approach for quantifying analytes without the need for complex equipment and high-cost reagents [17,18]. In particular, nanozymes such as carbon [19], metal [20], or metal oxide [21] nanomaterials could oxidize the colorless TMB into blue oxTMB with the help of hydrogen peroxide (H_2O_2). However, these systems require H_2O_2 as a substrate. H_2O_2 is very sensitive to the surrounding environment, and the identification of suitable storage for direct point-of-care detection is difficult.

As one kind of redox active two-dimensional (2D) nanosheets, MnO_2 nanosheets have attracted considerable interests for their unique properties, including low cost, high specific surface area, good chemical stability, nontoxicity and abundant availability. Recently, MnO_2 nanosheets were found to exhibit intrinsic oxidase like activity due to the presence of oxygen defect [22]. MnO_2 can not only oxidize colorless TMB into blue oxidized product (oxTMB) without the requirement of H_2O_2 but also oxidize a great deal of reducing substrates, thus providing promising opportunities for advanced development of the colorimetric assay. For example, Wan et al. fabricated a colorimetric immunosensing platform for quantitative detection of toxicological substrates in complicated systems based on MnO_2 [22]. Liu et al. described a rapid and highly sensitive colorimetric assay for the detection of glutathione (GSH) employing MnO_2 nanosheets as an artificial oxidase [23]. He et al. reported a unique visual colorimetric sensor array for discrimination of antioxidants in serum based on MnO_2 nanosheets-TMB multicolor chromogenic system [24]. Besides, the system could be applied to quantitatively measure other inhibitor of TMB oxidation including H_2O_2 and glucose in blood, single stranded DNA, and ascorbic acid [25–27]. Recently, Lin et al. constructed a colorimetric sensing platform for quantitative detection of acetylcholinesterase (AChE) activity and inhibitor [28]. As far as we know, there are few reports about the detection strategy which combined the specificity of enzyme and the MnO_2 nanosheets catalyzed visual detection.

In the present work, it was discovered that NADH could efficiently decompose MnO_2 nanosheets to generate Mn^{2+}, while NADH could be oxidized into NAD^+. Due to the decomposition of MnO_2 nanosheets, TMB would not be oxidized, resulting in the decrease of absorbance intensity at 652 nm, which is thus employed to quantitatively detect NADH. Considering that numerous redox enzymes use the common NADH/NAD^+ cofactor, the colorimetric analysis of NADH can provide a generic method to analyze NADH/NAD^+-dependent enzyme activities, as well as to detect their reaction substrates. Herein, the proposed method has been validated by using alcohol dehydrogenase (ADH) and lactate dehydrogenase (LDH) catalyzed physiological reactions. As shown in Scheme 1, ethanol and NAD^+ cofactor could react to form acetaldehyde and NADH in the presence of ADH. Thus, the absorbance intensity of MnO_2-TMB system would be decreased in the presence of ethanol due to the formation of NADH by the enzyme-catalyzed reaction. In contrast, pyruvic acid and NADH cofactor could react to form lactic acid and NAD^+ in the presence of LDH. The absorbance intensities of MnO_2-TMB system could easily decrease in the presence of NADH, and then it would be recovered with the increasing amounts of pyruvic acid in the presence of LDH due to the consumption of NADH by the enzyme-catalyzed reaction. Therefore, a simple method was successfully developed for the highly sensitive and selective detection of ethanol and pyruvic acid, respectively.

2. Experimental

2.1. Materials and instruments

All reagents used were of analytical grade unless otherwise indicated. Manganese (II) chloride tetrahydrate ($MnCl_2{\cdot}4H_2O$), 3,3′,5,5′-tetramethylbenzidine (TMB), sodium dehydrogenized phosphate (NaH_2PO_4), disodium hydrogen phosphate (Na_2HPO_4), tetramethylammonium hydroxide (TMA·OH), peroxide hydrogen (H_2O_2) and other salts were purchased from Aladdin Reagent Co. Ltd. (Shanghai, China). NADH, NAD^+, ethanol dehydrogenase (ADH, EC 1.1.1.1) from baker's yeast in the form of lyophilized powder, lactate dehydrogenase (LDH), pyruvic acid, and lactic acid were purchased from Sigma-Aldrich Corporation.

Transmission electron microscope (TEM) images were obtained using a Philips CM200 FEG microscope. X-ray photoelectron spectroscopy (XPS) analysis was performed using X-ray photoelectron spectrometer model ESCALAB 250 with an AlKa X-ray source (Thermo, USA). Raman spectra were carried out with a HR 800 Raman spectrometer with an excitation laser at 633 nm (Horiba, France). The UV–vis absorption spectra were recorded on a UV–vis spectrophotometer (Shimadzu, UV-3600, Japan). The desired pH buffer solutions were adjusted with pHS-3C pH meter (Shanghai, China).

2.2. Preparation of MnO_2 nanosheets

MnO_2 nanosheets were prepared according to the previously reported method [29]. In a typical synthesis process, 8 mL of 1.0 M TMA·OH and 1.5 mL H_2O_2 were mixed and then diluted to 15 mL ultrapure water. After that, the solution was mixed with 0.415 g $MnCl_2{\cdot}4H_2O$ within 30 s. The mixture was stirred vigorously overnight and MnO_2 nanosheets were obtained from the suspension by centrifugation at 10,000 rpm for 10 min, followed by washing three times with methanol. Afterwards, MnO_2 nanosheets were washed three times with deionized water. To obtain homogeneous MnO_2 nanosheets solution, the as-prepared MnO_2 samples were further treated by a SCIENTZ-IID ultrasonic homogenizer (Ningbo Scientz Biochenology Co. Ltd. China).

2.3. UV–vis measurements

In a typical NADH assay, 10 μL different concentrations of NADH, and 30 μL MnO_2 nanosheets solution were added into a centrifuge tube containing 420 μL 10 mM PBS buffer with pH of 5.0. After incubation for 10 min to ensure complete reaction, 40 μL of 5.0 mM TMB was added into the above mixture solution and mixed for 10 min at room temperature. The UV–vis spectra were recorded from 550 nm to 750 nm. Absorbance at 652 nm of solution was collected for analysis.

For the analysis of ethanol, 30 μL of NAD^+ (10 mM), 10 μL of ADH (1.0 mg/mL), and 20 μL of different concentrations of ethanol were mixed with 20 μL of PBS (pH = 9.0, 10 mM). After incubated at 37 °C for 20 min, 40 μL of TMB solution (5.0 mM), 30 μL of MnO_2 nanosheets, and 350 μL of PBS buffer (pH = 5.0, 10 mM) were added. Subsequently, the solution was incubated for 10 min before the absorption spectra were collected. Absorbance (652 nm) of solution was collected for analysis.

For the analysis of pyruvic acid, 15 μL of NADH (5.0 mM), 10 μL of LDH (1.0 mg/mL), and 50 μL of different concentrations of pyruvic acid were mixed with 30 μL PBS buffer (pH = 6.0, 10 mM). After incubated at 37 °C for 10 min, 40 μL of TMB solution (5.0 mM), 30 μL of MnO_2 nanosheets, and 325 μL of PBS buffer (pH = 5.0, 10 mM) were added successively into the above mixture followed by the thoroughly shaking and equilibrated for 10 min. Finally, the UV–vis absorption spectra were measured by spectrophotometer.

2.4. Preparation of real samples

Commercial alcoholic beverage samples were diluted with 10 mM PBS in appropriate concentration and then analyzed with the proposed analysis method.

The commercial calcium pyruvate tablets were thoroughly grinded using agate mortar. The resulting powder were weighted, dissolved by

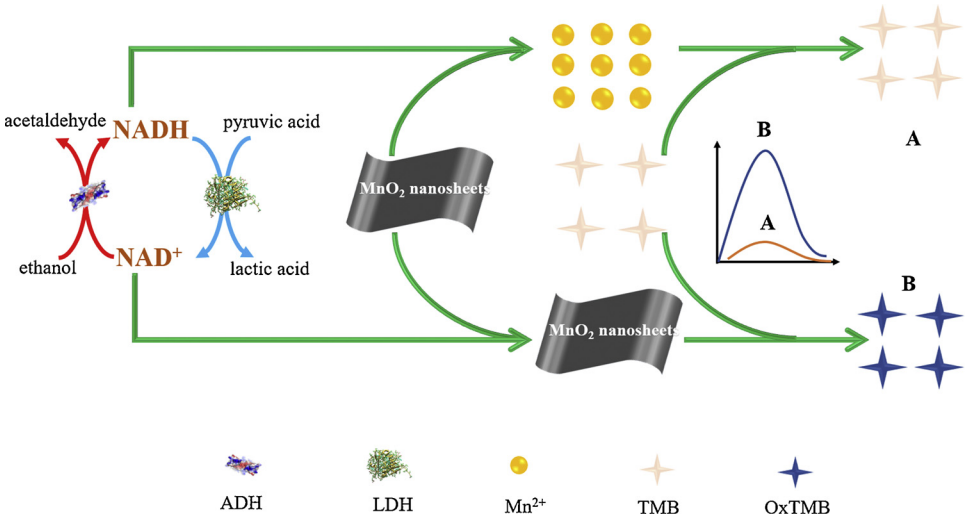

Scheme 1. The schematic of colorimetric sensing platform for probing the NAD^+/NADH -dependent biocatalytic transformations based on MnO_2-TMB system.

distillation water, filtrated, and then made to constant volume. The obtained calcium pyruvate tablet solution was further diluted to an appropriate concentration for the next colorimetric detection.

3. Results and discussion

3.1. Characterization of MnO_2 nanosheets

In this work, the MnO_2 nanosheets were synthesized by oxidation of Mn^{2+} with H_2O_2 in the presence of TMA·OH. The resulting MnO_2 nanosheets were systematically characterized by TEM, Raman spectrum and XPS. As shown in Fig. 1A, the MnO_2 nanosheets exhibited a large 2D and ultrathin plane with occasional folds and crinkles, indicating that the nanostructures possessed a large surface area for the reaction with TMB. The Raman shift at 567 cm^{-1} and 653 cm^{-1} can be attributed to the Mn—O vibration [30] (Fig. 1B). XPS was used to make a qualitative analysis of chemical valence and binding of the elements for the obtained MnO_2. Two characteristic peaks centered at 641.0 eV and 652.8 eV were observed, belonging to $Mn_{2p3/2}$ and $Mn_{2p1/2}$, respectively [31] (Fig. 1C). Another peak centered at 528.6 eV was observed, corresponding to the O_{1s} (Fig. 1D). These results further supported the successful preparation of MnO_2 nanosheets.

3.2. Fabrication and principle of visual colorimetric sensor assay for NADH

It was well recognized in the previous reports [23–28], MnO_2 can possess oxidase-like catalysis activity. To further verify the capacity of MnO_2 nanosheets, MnO_2 nanosheets were employed for the direct incubation with TMB to catalyze colorimetric reaction. As shown in Fig. 2A, TMB had no clear absorption peaks from 550 nm to 750 nm

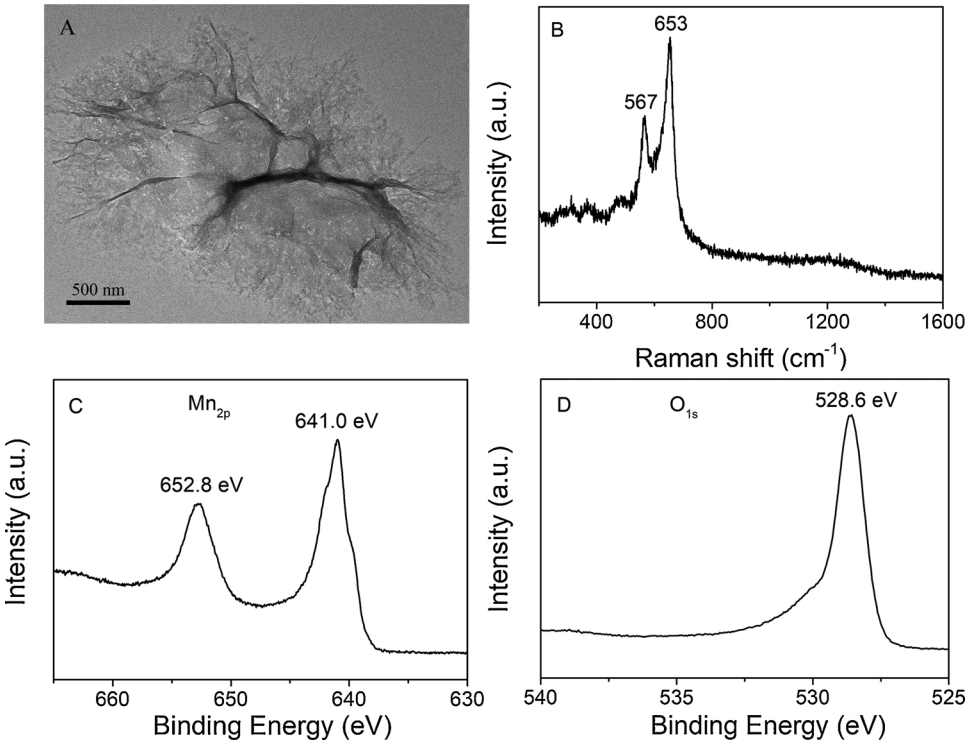

Fig. 1. The TEM image (A), Raman spectrum (B), XPS spectra of Mn_{2p} (C) and XPS spectra of O_{1s} (D).

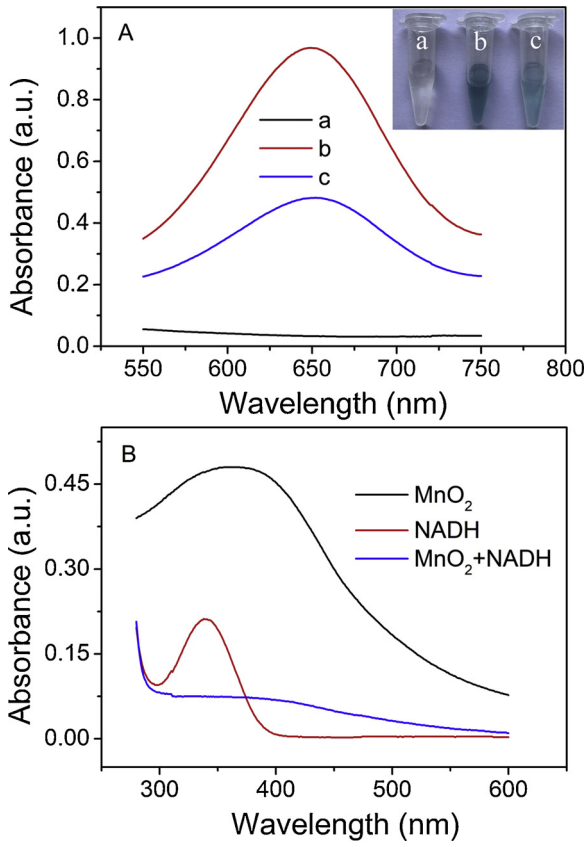

Fig. 2. (A) UV–vis absorption spectra of TMB (a), and TMB incubated with MnO_2 nanosheets in the absence (b) and presence (c) of NADH. (Inset: photographs of the corresponding product solutions). (B) UV–vis absorption spectra of the MnO_2 nanosheets, NADH, and MnO_2 nanosheets incubated with NADH. [TMB] = 0.40 mM, [NADH] = 50 μM. (For interpretation of the references to colour in the text, the reader is referred to the web version of this article.)

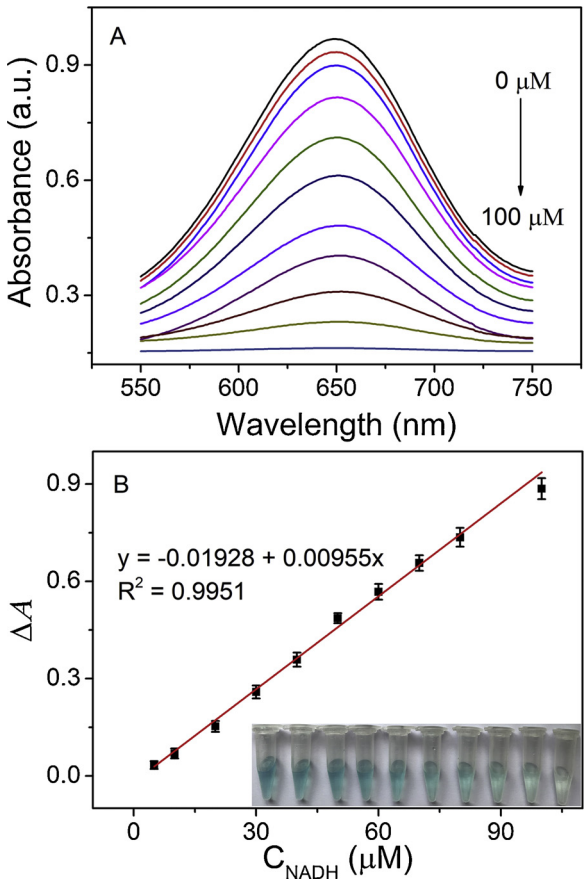

Fig. 3. (A) The UV–vis absorption spectra of MnO_2-TMB system in the presence of different concentrations of NADH. (B) The NADH calibration plot. Inset: the corresponding digital photos.

(curve a). Yet, there was a strong absorption peak at 652 nm after the mixture of MnO_2 and TMB (curve b). Moreover, the solution color has been changed from colorless to blue (Inset), indicating that MnO_2 nanosheets could possess the oxidase-like catalysis activity. However, after the addition of NADH into the MnO_2-TMB system, the absorbance at 652 nm decreased obviously with the blue color fading (curve c). This may be attributed to the fact that NADH can trigger the decomposition of MnO_2 nanosheets. Due to the decomposition of MnO_2 nanosheets, TMB would not be oxidized followed by the decrease of absorbance intensity at 652 nm.

The interaction between MnO_2 and NADH was confirmed by testing the UV–vis spectra of MnO_2 nanosheets in the presence and absence of NADH. As shown in Fig. 2B, the characteristic peak of the MnO_2 nanosheets at 380 nm decreased after incubation with NADH, indicating that MnO_2 nanosheets could be reduced to Mn^{2+} by NADH, although the direct reduction of oxTMB by NADH cannot be excluded. As a control, the presence of NAD^+ presented a negligible influence on the UV–vis spectra of MnO_2 (Fig. S1). Moreover, the distinct UV–vis absorbance band centered at 340 nm of NADH decreased obviously after the incubation with MnO_2, indicating that NADH could be oxidized to NAD^+ by MnO_2. As shown in Eq. (1), MnO_2 nanosheets were reduced to produce Mn^{2+}.

$$MnO_2 + NADH + 3H^+ \rightarrow Mn^{2+} + NAD^+ + 2H_2O \quad (1)$$

In addition, the TEM images of MnO_2 nanosheets in the presence of NADH and NAD^+ were investigated (Fig. S2). As shown in Fig. S2A, after incubation with NADH, the plane structure of MnO_2 was destroyed due to the decomposition of MnO_2 nanosheets by NADH. In contrast, the presence of NAD^+ had negligible influence on the morphology of MnO_2 (Fig. S2B). These results indicated that NADH-induced decomposition of MnO_2 nanosheets could serve as an accurate probe for NADH in solution.

3.3. Detection of NADH

In order to obtain a better sensing performance for NADH detections, several experimental conditions were optimized prior to the application of this method, such as the reaction time, pH values, the volumes of MnO_2, and the concentrations of TMB. The absorbance difference $\Delta A = A_0 - A$, where A_0 and A was the absorbance of MnO_2-TMB system in the absence and presence of NADH, respectively, was used the criteria to select the optimal conditions. As shown in Fig. S3, the reaction between TMB and MnO_2 could be completed within 10 min; the optimal pH value was 5.0; the optimal volume of MnO_2 was 30 μL; and the ideal concentration of TMB was 0.4 mM. The following experiments were performed under the optimal conditions.

Under the optimal conditions, NADH was analyzed by the MnO_2-TMB-based sensing platform. As shown in Fig. 3A, along with the concentrations increasing from 5 to 100 μM, the absorbance intensities of MnO_2-TMB system displayed the continuous decreases. Meanwhile, Fig. 3B illustrated an excellent linear relationship between ΔA and the NADH concentrations. The regression equation was obtained as $\Delta A = -0.01928 + 0.00955\ C_{NADH}$ (μM) ($R^2 = 0.9951$). Moreover, the color changes of MnO_2-TMB system in the presence of various amounts of NADH were recorded by using a digital camera (Inset of Fig. 3B). The color change of MnO_2-TMB system induced by NADH can be visualized by the naked eye. These results show that the developed MnO_2-TMB system is suitable for the NADH detection. Moreover, the platform has a

great potential for monitoring the enzyme catalysis of two different dehydrogenase models, ADH and LDH, where NADH is formed and consumed, respectively, in their physiological enzymatic reactions.

3.4. Probing the ADH-catalyzed biocatalytic transformation

The ability of analyzing the NADH cofactor with the MnO_2-TMB system also enabled the use of this system to study the activity of NAD^+-dependent enzymes as well as their substrates. As a model system, the MnO_2-TMB system was separately applied to analyze NAD^+-dependent ADH and the substrate ethanol. The reaction principle was based on the following equation:

$$\text{Ethanol} + NAD^+ \rightarrow \text{Acetaldehyde} + NADH + H^+ \text{ (in the presence of ADH)} \quad (2)$$

As shown in Scheme1, in the presence of ADH, ethanol could react with NAD^+ to generate NADH, which induced the absorbance intensity decrease of MnO_2-TMB system. Control experiments revealed that no decrease of the absorbance intensity occurred in the presence of ethanol, NAD^+, ADH, ethanol with NAD^+, ethanol with ADH, and NAD^+ with ADH, respectively (Fig. S4). These results indicated that the decrease of absorbance intensity of MnO_2-TMB system originated from the ADH/ethanol-generated NADH. Thus, this photophysical process enabled the quantitative assay of ADH as well as ethanol.

By retaining the concentrations of NAD^+ and ethanol in the system constant, except the concentration of ADH, the biocatalytic reactions in the system was allowed to proceed for a fixed time. It was found that the resulting absorbance decrease of MnO_2-TMB system related directly to the concentration of ADH (Fig. S5). Fig. S5A showed the absorbance responses of MnO_2-TMB system upon the addition of different concentrations of ADH. The calibration curve was shown in Fig. S5B. ADH can be detected as low as 0.0050 μg/mL (1.5 mU/mL).

Similarly, the MnO_2-TMB system was also applied for the quantitative detection of ethanol (Fig. 4). Fig. 4A depicted the absorption spectra of MnO_2-TMB system resulting from the activation of biocatalyzed oxidation of ethanol and the generation of NADH. As the concentration of ethanol increased, the absorbance intensities of MnO_2-TMB system decreased, in consistence with the higher-content generation of NADH. The derived calibration curve was presented in Fig. 4B. There was a good linear relationship between the ΔA and ethanol concentrations in the range of 0.010–1.0 mM and 1.0–10 mM. The regression equation could be described as follow: $\Delta A = 0.05505 + 0.1369\ C$ (mM) and $\Delta A = 0.1375 + 0.0661\ C$ (mM), with corresponding regression coefficient of 0.9966 and 0.9971, respectively. The detection limit for ethanol was 5.0 μM. The color change of MnO_2-TMB system induced by ethanol can be visualized by the naked eye (Inset of Fig. 4B). The standard deviation for six replicate measurements of 0.50 mM and 5.0 mM ethanol was obtained to be 3.41% and 2.69%, respectively. Compared with the previous reports on the detections of ethanol (Table 1), the developed MnO_2-TMB-based colorimetric method could achieve the lower detection limit and wider linear range for the determination of ethanol.

The selectivity for the ethanol detection was further investigated by using various other interferents. As shown in Fig. S6, among a series of potentially interfering organic compounds including methanol, propanol, isopropanol, cyclohexanol, tertiary butanol, *n*-butyl alcohol, benzyl alcohol, only ethanol could effectively decrease the absorbance of the MnO_2-TMB system. In contrast, the other organic molecules nearly had no effect on the absorbance of MnO_2-TMB system. The results indicated that the selectivity of this method was acceptable.

In order to estimate the applicability of this method, the developed ethanol biosensor was applied for the analysis of ethanol in alcoholic beverages including commercial red wine, dark beer and spirit samples. The results are shown in Table S1. It can be seen that the results obtained with the developed biosensor were in good agreement with those certified by the supplier.

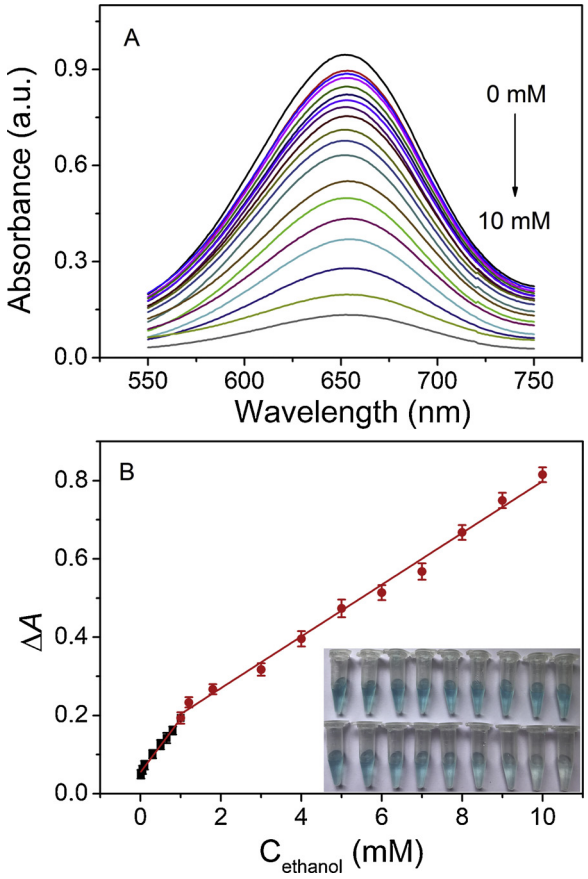

Fig. 4. (A) The UV–vis absorption spectra of MnO_2-TMB system with different concentrations of ethanol (from 0 to 10 mM). (B) The linear plot of ΔA versus the concentrations of ethanol (0.010, 0.050, 0.10, 0.30, 0.50, 0.65, 0.80, 1.0, 1.2, 1.8, 3.0, 4.0, 5.0, 6.0, 7.0, 8.0, 9.0 and 10 mM). Inset: the corresponding photos. [TMB] = 0.40 mM, [NAD^+] = 0.60 mM, [ADH] = 20 μg/mL.

3.5. Probing the LDH-catalyzed biocatalytic transformation

The ability of MnO_2-TMB system in analyzing the NADH cofactor was explored by studying the activity of NADH-dependent enzymes as well as their substrates. As a model system, the MnO_2-TMB system was applied to analyze NADH-dependent LDH and the substrate of pyruvic acid. The reaction principle was based on the following equation:

$$\text{Pyruvic acid} + NADH \rightarrow \text{Lactic acid} + NAD^+ \text{ (in the presence of LDH)} \quad (3)$$

As shown in Scheme 1, we designed the MnO_2-TMB platform to probe the LDH-catalyzed transformation based on the different responses of NADH and NAD^+ towards the MnO_2-TMB system and the enzyme-catalyzed reaction system. Firstly, the feasibility of the developed MnO_2-TMB system for probing the LDH-dependent biocatalytic transformation was assessed with the results shown in Fig. S7. The UV–vis absorption spectra of MnO_2-TMB system under different conditions were recorded. As shown in Fig. S7, the MnO_2-TMB system had a strong absorption peak centered at 652 nm, which could decrease in the presence of NADH due to the decomposition of NADH towards MnO_2. The absorbance intensity of MnO_2-TMB-NADH system could not be influenced by pyruvic acid or LDH. When both pyruvic acid and LDH existed, the absorbance intensity at 652 nm resorted efficiently, indicating the consumption of NADH. Therefore, the MnO_2-TMB-NADH system could be used to follow the activity of LDH as well as quantitatively detect pyruvic acid.

Table 1
Comparison of different analysis methods for the determination of ethanol.

Methods	Probe/Materials/Reagents (used)	Linear range	Detection limit	Refs.
Amperometry	Acid fuchsin adsorbed onto zirconia nanotubes	0.05–7.5 mM	25 μM	[32]
	niobium oxide/Meldola's blue/silica gel	0.1–10 mM	8 μM	[33]
Potentiometry	microbial	0.02–50 mM	–	[34]
Fluorescence	Trypsin-stabilized Ag nanoclusters	10–300 μM	5 μM	[35]
Colorimetry	Formazan	1–5 mM	–	[36]
	Acidic ceric nitrate	0.1–10% (V/V)	0.03% (V/V)	[37]
	Based on MnO_2-TMB system	0.01–1.0 mM 1.0–10 mM	5.0 μM	This work

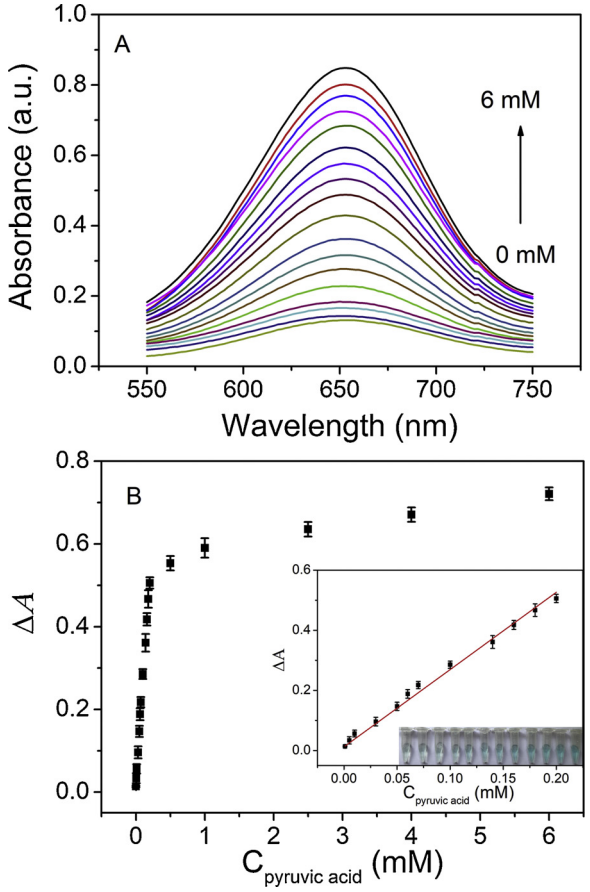

Fig. 5. (A) The UV–vis absorption spectra of MnO_2-TMB-NADH system with different concentrations of pyruvic acid (from 0 to 6 mM). (B) The change trend of the Δ*A* with different concentrations of pyruvic acid, inset showed the linear plot of Δ*A* versus the low concentration of pyruvic acid (1.0, 5.0, 10, 30,50, 60, 70,100, 140, 160, 180, and 200 μM). Inset: the corresponding photos. [TMB] = 0.40 mM, [NADH] = 50 μM, [LDH] = 20 μg/mL.

Fig. S8A showed the absorbance responses of the MnO_2-TMB-NADH system upon the addition of different concentrations of LDH. The calibration curve was shown in Fig. S8B. LDH can be detected as low as 0. 50 ng/mL (0.050 mU/mL). Fig. 5 depicted the absorbance intensities of the MnO_2-TMB-NADH system resulting from the activation of biocatalyzed reduction of pyruvic acid and the consumption of NADH. As the concentration of pyruvic acid increased, the absorbance intensities of MnO_2-TMB-NADH system increased, consistent with the higher content of pyruvic acid. The derived calibration curve was presented in Fig. 5B. There was a good linear relationship between the Δ*A* and pyruvic acid concentration in the range of 1.0–200 μM. The regression equation could be described as follow: $\Delta A = 0.0122 + 2.571C_{\text{puruvic acid}}$ (μM). The corresponding regression coefficient was 0.9978, and the detection limit for pyruvic acid was 100 nM. Moreover, the color change of the MnO_2-TMB-NADH system induced by pyruvic acid can be visualized by the naked eye (Inset of Fig. 5B). The standard deviation for six replicate measurements of 10.0 μM pyruvic acid was 3.12%. Compared with the previous reports on the detections of pyruvic acid shown in Table 2, our method based on the MnO_2-TMB-NADH system for the determination of pyruvic acid obtained the lower detection limit and wider linear range.

The selectivity for pyruvic acid detection was further investigated by using various other interferents. As shown in Fig. S9, among a series of potentially interfering molecules and ions, only pyruvic acid molecule could effectively restore the absorbance of the MnO_2-TMB-NADH system. Accordingly, the other molecules or ions nearly had no effect on the absorbance of MnO_2-TMB-NADH system. The results indicated that the selectivity of this method was acceptable.

To demonstrate this method was feasible, it was applied to the determination of pyruvic acid in commercial calcium pyruvate tablets. The tablets were diluted appropriately to bring them to their working concentration range. As shown in Table S2, the recoveries of known amounts of pyruvic acid were in the range 93.0–105.2% with RSD ranging from 2.12% to 3.49%. The results demonstrated the potential applicability of the MnO_2-TMB-NADH system for the detection of pyruvic acid content in commercial tablets.

4. Conclusion

The present study has developed a MnO_2-TMB-based sensing platform for monitoring the biocatalytic transformations. This sensing platform relies on the catalytic ability of MnO_2 nanosheets to directly oxidize TMB into oxTMB. We demonstrated that NADH could trigger the decomposition of MnO_2 nanosheets, resulting the weaken progression of MnO_2-TMB platform in the visual color, which enabled the probing of the dehydrogenase-stimulated NADH-generating or

Table 2
Comparison of different analysis methods for the determination of pyruvic acid.

Methods	Probe/Materials/Reagents(used)	Linear range	Detection limit	Refs.
Amperometry	Poly(mercapto-p-benzoquinone) film	0–2 mM	1 μM	[38]
	A bienzyme modified carbon paste electrode	0–5 mM	5 μM	[39]
	Covalent attachment to polytyramine	0.1–3 mM	0.05 mM	[40]
Fluorescence	NADH as fluorescence probe with LDH	0.2–1.2 mM	12 μM	[41]
	LDH as fluorescence probe	3.0–25 μM	0.88 μM	[42]
Colorimetry	Dinitrophenylhydrazine	0–10 mM	0.5 mM	[43]
	MnO_2-TMB-NADH system	1.0–200 μM	100 nM	This work

consuming bio-transformations. This was exemplified with the analysis of the ADH-mediated oxidation of ethanol and the LDH-mediated reduction of pyruvic acid. So that the selective detections of ethanol and pyruvic acid could be separately expected with high sensitivity. Importantly, the proposed method may pave the way to implement the MnO_2-TMB as the optical labels to follow the activity of other dehydrogenase and their substrates.

Acknowledgements

This work is kindly supported by the National Natural Science Foundation of China (Nos. 21405094, 21775088, and 21675099), the Natural Science Foundation of Qinghai Province of China (2016-ZJ-955), and the Development Project of Qinghai Key Laboratory (No. 2017-ZJ-Y10), the Open Funds of Shandong Key Laboratory of TCM Quality Control Technology of Shandong Academy of Sciences, and the Scientific Research Foundation of Qufu Normal University (No. BSQD201203).

Appendix A. Supplementary data

Supplementary material related to this article can be found, in the online version, at doi:https://doi.org/10.1016/j.snb.2018.11.140.

References

[1] Z.Q. Gao, K.C. Deng, X.D. Wang, M. Miro, D.P. Tang, High-resolution colorimetric assay for rapid visual readout of phosphatase activity based on gold/silver core/shell nanorod, ACS Appl. Mater. Interfaces 6 (2014) 18243–18250.
[2] W.H. Ying, NAD^+/NADH and $NADP^+$/NADPH in cellular functions and cell death: regulation and biological consequences, Antioxid. Redox Signal. 10 (2008) 179–206.
[3] R. Freeman, T. Finder, L. Bahshi, I. Willner, β-Cyclodextrin-modified CdSe/ZnS quantum dots for sensing and chiro-selective analysis, Nano Lett. 9 (2009) 2073–2076.
[4] R. Freeman, R. Gill, I. Shweky, M. Kotler, U. Banin, I. Willner, Bio-sensing and probing of intracellular metabolic pathways by NADH-sensitive quantum dots, Angew. Chem. Int. Ed. 48 (2009) 309–313.
[5] G. Aragay, F. Pino, A. Merkoci, Nanomaterials for sensing and destroying pesticides, Chem. Rev. 112 (2012) 5317–5338.
[6] I. Willner, B. Willner, Biomolecule-based nanomaterials and nanostructures, Nano Lett. 10 (2010) 3805–3815.
[7] F. Wang, X. Liu, I. Willner, Integration of photoswitchable proteins, photosynthetic reaction centers and semiconductor/biomolecule hybrids with electrode supports for optobioelectronic applications, Adv. Mater. 25 (2013) 349–377.
[8] N.L. Rosi, C.A. Mirkin, Nanostructures in biodiagnostics, Chem. Rev. 105 (2005) 1547–1562.
[9] K. Saha, S.S. Agasti, C. Kim, X. Li, V.M. Rotell, Gold nanoparticles in chemical and biological sensing, Chem. Rev. 112 (2012) 2739–2779.
[10] R.D. Larica, R.M. Fratila, A. Szarpak, J. Huskens, A.H. Velders, Multivalent nanoparticle networks as ultrasensitive enzyme sensors, Angew. Chem. Int. Ed. 50 (2011) 5704–5707.
[11] B.K. Jena, C.R. Raj, Electrochemical biosensor based on integrated assembly of dehydrogenase enzymes and gold nanoparticles, Anal. Chem. 78 (2006) 6332–6339.
[12] B. Shlyahovsky, E. Katz, Y. Xiao, V. Pavlov, I. Willner, Optical and electrochemical detection of NADH and of NAD^+ dependent biocatalyzed processes on gold nanoparticles, Small 2 (2005) 213–216.
[13] M. Zayats, S.P. Pogorelova, A.B. Kharitonov, O. Lioubashevski, E. Katz, I. Willner, Au nanoparticle-enhanced surface plasmon resonance sensing of biocatalytic transformations, Chem. Eur. J. 9 (2003) 6108–6114.
[14] R. Freeman, R. Gill, I. Shweky, M. Kotler, U. Banin, I. Willner, Biosensing and probing of intracellular metabolic pathways by NADH-sensitive quantum dots, Angew. Chem. Int. Ed. 48 (2009) 309–313.
[15] U.S. Akshath, P. Bhatt, Tunneling of redox enzymes to design nano-probes for monitoring NAD^+ dependent bio-catalytic activity, Biosens. Bioelectron. 85 (2016) 240–246.
[16] Y.F. Yuan, K. Huang, M.F. Chang, C.F. Qin, S.J. Zhang, H.F. Pan, Y. Chen, J.H. Xu, Dual emission fluorescent silver nanoclusters for sensitive detection of the biological coenzyme NAD^+/NADH, Anal. Biochem. 494 (2016) 46–48.
[17] C.T. Wu, D.Q. Fan, C.Y. Zhou, Y.Q. Liu, E.K. Wang, Colorimetric strategy for highly sensitive and selective simultaneous detection of histidine and cysteine based on G-quadruplex-Cu(II) metalloenzyme, Anal. Chem. 88 (2016) 2899–2903.
[18] C.H. Lei, X.E. Zhao, J. Sun, X.L. Yan, Y. Gao, H. Gao, S.Y. Zhu, H. Wang, A simple and novel colorimetric assay for tyrosinase and inhibitor screening using 3,3′,5,5′-tetramethylbenzidine as a chromogenic probe, Talanta 175 (2017) 457–462.
[19] S.Y. Zhu, X.E. Zhao, J.M. You, G.B. Xu, H. Wang, Carboxylic-group-functionalized single-walled carbon nanohorns as peroxidase mimetics and their application to glucose detection, Analyst 140 (2015) 6398–6403.
[20] T. Jiang, Y. Song, T.X. Wei, H. Li, D. Du, M.J. Zhu, Y.H. Lin, Sensitive detection of Escherichia coli O157:H7 using Pt-Au bimetal nanoparticles with peroxidase-like amplification, Biosens. Bioelectron. 77 (2016) 687–694.
[21] H. Wei, E.K. Wang, Fe_3O_4 magnetic nanoparticles as peroxidase mimetics and their applications in H2O2 and glucose detection, Anal. Chem. 80 (2008) 2250–2254.
[22] Y. Wang, P. Qin, D. Zhang, J. Wu, Y. Wang, Manganese oxide nanowire-mediated enzyme-linked immunosorbent assay, Biosens. Bioelectron. 33 (2012) 69–74.
[23] J. Liu, L.J. Meng, Z.F. Fei, P.J. Dyson, X.N. Jing, X. Liu, MnO_2 nanosheets as an artificial enzyme to mimic oxides for rapid and sensitive detection of glutathione, Biosens. Bioelectron. 90 (2017) 69–74.
[24] W. Huang, Y.Q. Deng, Y. He, Visual colorimetric sensor array for discrimination of antioxidants in serum using MnO_2 nanosheets triggered multicolor chromogenic system, Biosens. Bioelectron. 91 (2017) 89–94.
[25] J. Yuan, Y. Cen, X.J. Kong, S. Wu, C.L. Liu, R.Q. Yu, X. Chu, MnO_2-nanosheet-modified up-conversion nanosystem for sensitive turn-on fluorescence detection of H_2O_2 and glucose in blood, ACS Appl. Mater. Interfaces 7 (2015) 10548–10555.
[26] L. Lin, D.M. Shi, Q.F. Li, G.F. Wang, X.J. Zhang, Detection of T4 polynucleotide kinase based on a MnO_2 nanosheet-3,3',5,5' -tetramethylbenzidine (TMB) colorimetric system, Anal. Methods 8 (2016) 4119–4126.
[27] H.L. Yu, L. Zheng, Manganese dioxide nanosheets as an optical probe for photometric determination of free chlorine, Microchim. Acta 183 (2016) 2229–2234.
[28] X. Yan, Y. Song, X.L. Wu, C.Z. Zhu, X.G. Su, D. Du, Y.H. Lin, Oxidase-mimicking activity of ultrathin MnO_2 nanosheets in colorimetric assay of acetylcholinesterase activity, Nanoscale 6 (2017) 2317–2323.
[29] Z.M. Huang, Q.Y. Cai, D.C. Ding, J. Ge, Y.L. Hu, J. Yang, L. Zhang, Z.H. Li, A facile label-free colorimetric method for highly sensitive glutathione detection by using manganese dioxide nanosheets, Sens. Actuators B: Chem. 242 (2017) 355–361.
[30] G. Zhao, J. Li, L. Jiang, H. Dong, X. Wang, W. Hu, Synthesizing MnO_2 nanosheets from graphene oxide templates for high performance pseudosupercapacitors, Chem. Sci. 3 (2012) 433–437.
[31] L. Peng, X. Peng, B. Liu, C. Wu, Y. Xie, G. Yu, Ultrathin two-dimensional MnO_2/graphene hybrid nanostructures for high-performance, flexible planarsupercapacitors, Nano Lett. 13 (2013) 2151–2157.
[32] X.Q. Liu, B.H. Li, M. Ma, G.Q. Zhan, C.X. Liu, C.Y. Li, Amperometric sensing of NADH and ethanol using a hybrid film electrode modified with electrochemically fabricated zirconia nanotubes and poly (acid fuchsin), Mircochim. Acta 76 (2012) 123–129.
[33] A.S. Santos, R.S. Freire, L.T. Kubota, Highly stable amperometric biosensor for ethanol based on Meldola's blue adsorbed on silica gel modified with niobium oxide, J. Electroanal. Anal. Chem. 547 (2003) 135–142.
[34] L. Rotariu, C. Bala, V. Magearu, New potentiometric microbial biosensor for ethanol determination in alcoholic beverages, Anal. Chim. Acta 513 (2004) 119–123.
[35] S.Y. Liu, H. Wang, Z. Cheng, H.G. Liu, Facile synthesis of near infrared fluorescent trypsin-stabilized Ag nanoclusters with tunable emission for 1,4-dihydronicotinamide adenine dinucleotide and ethanol sensing, Anal. Chim. Acta 886 (2015) 151–156.
[36] J.P. Zanon, M.F.S. Peres, E.A.L. Gattas, Colorimetric assay of ethanol using alcohol dehydrogenase from dry baker's yeast, Enzyme Microbial Technol. 40 (2007) 466–470.
[37] P. Pinyou, N. Youngvises, J. Jakmunee, Flow injection colorimetric method using acidic ceric nitrate as reagent for determination of ethano, Talanta 84 (2011) 745–751.
[38] G. Arai, T. Noma, H. Habu, I. Yasumori, Pyruvate sensor based on pyruvate oxidase immobilized in a poly (mercapto-*p*-benzoquinone) film, J. Electroanal. Chem. 464 (1999) 143–148.
[39] W. Bergmann, R. Rudolph, U. Sphon, A bienzyme modified carbon paste electrode for amperometric detection of pyruvate, Anal. Chim. Acta 394 (1999) 233–241.
[40] M. Situmorang, J.J. Gooding, D.B. Hibbert, D. Barnett, The development of a pyruvate biosensor using electrodeposited polytyramine, Electroanalysis 14 (2002) 17–21.
[41] Y.Y. Zhao, G.F. Gao, Y.S. Li, X. Ju, J. Zhang, J. Zheng, Determination of pyruvic acid by using enzymatic fluorescence capillary analysis, Talanta 76 (2008) 65–70.
[42] S. Marcos, J. Galban, C. Alonso, J.R. Castillo, Intrinsic molecular fluorescence of lactate dehydrogenase: an analytical alternative for enzymic determination of pyruvate, Analyst 122 (1997) 355–395.
[43] K.S. Yoo, L.M. Pike, B.K. Hamilton, A simplified pyruvic acid analysis suitable for onion breeding programs, Hortic. Sci. 30 (1999) 1306.

Shuyun Zhu received her PhD from Changchun Institute of Applied Chemistry in 2012, and now is working at Qufu Normal University as an associate professor in Analytical Chemistry. Her current research interests include nanomaterials, as well as biosensors based on DNA and enzymes.

Cuihua Lei received her bachelor degree in Applied Chemistry from Weifang University in 2015, and now is a postgraduate student in Analytical Chemistry at Qufu Normal University. Her research interests focus on the synthesis and analytical application of carbon nanomaterials.

Jing Sun received his PhD from Northwest Institute of Plateau Biology in 2007, and now is working at Northwest Institute of Plateau Biology as an associate professor in Qinghai-Tibet Plateau Biological Resources. Her current research interests include quality control of Tibetan medicine and chemical analysis of resources.

Xian-En Zhao received his PhD from Northwest Institute of Plateau Biology in 2009, and

now is working at Qufu Normal University as an associate professor in Analytical Chemistry. His current research interests include biosensors, mass spectrometry analytical methodology, and pharmaceutical analysis.

Xiao Wang achieved his Ph.D. degree in Shandong Agriculture University. He is the director of Shandong Analysis and Test Center and Shandong Key Laboratory Breeding Base of Traditional Chinese Medicine Quality Control Technology. His current research interests include the quality control research of Traditional Chinese Medicine and the separation of active natural compounds.

Xiaolu Yan received her bachelor degree in Chemical Engineering and Technology from Qufu Normal University in 2016, and now is a postgraduate student in Analytical Chemistry at Qufu Normal University. Her research interests focus on the biosensors based on carbon nanomaterials and metal nanoclusters.

Wei Liu received his Ph.D. degree of plant nutriology at Huazhong Agriculture University in 2010. Then he worked as a researcher in Shandong Analysis and Test Center. His research interests focus on the cultivate and resources of Traditional Chinese Medicine.

Hua Wang received his Ph.D from Hunan University in 2004, and now is working at Qufu Normal University as a distinguished professor in Chemistry. His research interests mainly include chemical and biological sensors, advanced materials, and organic synthesis.